

## Experimental study of a granular flow in a vertical pipe: A spatiotemporal analysis

Jean-Luc Aider,\* Nathalie Sommier,† Tareck Raafat, and Jean-Pierre Hulin

*Laboratoire Fluides Automatique et Systèmes Thermiques, Bâtiment 502, Campus Universitaire, 91405 Orsay Cedex, France*

(Received 30 January 1998; revised manuscript received 5 October 1998)

The spatiotemporal characteristics of the flow of 125  $\mu\text{m}$  glass beads have been studied experimentally in a 2.9 mm diameter vertical glass pipe by means of a digital linear charge coupled device camera. The dynamics and propagation of granular density fluctuations have been analyzed in various flow regimes for different values of the granular mass-flow rate and of the degree of humidity  $H$ . At low flow rates, the granular flow has a high compactness and periodic intermittency effects occur at high  $H$  values: a pulsating bubble appears at the top of the flow channel and its time dependence is studied. At higher granular flow rates, a wave regime is observed with alternate low and high compactness regions: at low  $H$  values, the wave velocity is constant with time and can be measured precisely from the spatiotemporal diagrams. At higher humidity contents, periodic oscillations of the wave system are observed: at high amplitudes, transient blockages of the flow and a stick-slip displacement mode have been identified. [S1063-651X(99)06901-9]

PACS number(s): 81.05.Rm, 05.20.Dd, 83.70.Fn

### I. INTRODUCTION

Dry granular flows have become a widespread research topic in recent years, due both to their fundamental interest in relation to the physics of dispersed media and instabilities and to their many practical applications [1–4]. An enormous amount of granular materials must indeed be produced, transferred, and stored in various domains of activity such as the food industry, or civil and chemical engineering. A particularly important problem is the flow of granular materials in pipes observed in pneumatic transport applications or in the outflow of grains from storage silos. Such flows may display unwanted intermittency and/or blockage effects due to specific properties of granular materials such as the appearance of permanent vaults. This may result in large, dangerous, pressure transients and, in some cases, in a permanent clogging of the flow channels.

Similar phenomena have been observed at the scale of the laboratory in granular flows through circular tubes [5–9] or through hoppers of different angles [10]. In experiments in which a tube is attached to the outlet of the hopper [11], “shock-wave”-like patterns have been observed, propagating and interacting along the system in different ways. A great deal of theoretical work has been devoted to such problems of density fluctuations in granular flows [12–15]; these instabilities have, in particular, been discussed in terms of kinematic wave models [16,17] and traffic flow problems [18–20]. The occurrence of such density waves in pipes has also been demonstrated in numerical simulations using molecular dynamics or lattice-gas automata models [21–23].

In previous papers [7,8] we reported experimental studies of the flow of glass beads in small diameter vertical glass

pipes. In this very simple configuration, we have identified through optical transmission measurements a large variety of stationary or time dependent flow regimes. These studies allowed us to analyze the essential geometrical features of the various granular compact distributions and to determine the pressure profiles and fluctuations in these flows.

In the present paper we analyze experimentally the dynamical behavior of several of these granular flow patterns in the same experimental geometry: we use for that purpose spatiotemporal diagrams displaying time variations of the granular concentration distribution along the flow. Thanks to the large aspect ratio and the straight shape of the flow tube, these diagrams can be obtained conveniently by means of a linear digital charge coupled device (CCD) camera: it provides representative maps of the instantaneous grain density at a high repetition rate and with a good spatial resolution. This allows us to analyze fine scale details of the granular flow dynamics both in the space and in the time domains.

We concentrate the present study on flow regimes displaying significant dynamical effects. In the constant velocity wave regime, the spatiotemporal analysis allows us to study the buildup and disintegration of high density regions; the propagation velocity of the waves is also determined precisely. In the oscillating wave regime, variations of the oscillation amplitude with distance and complete blockage effects occurring at large oscillation amplitudes can be studied. In the compact flow regimes, a pulsating bubble may appear in the upper part of the flow tube: spatiotemporal diagrams help analyze the time variation of its length and give information on granular flow-rate variations inside it.

### II. EXPERIMENTAL PROCEDURE

Our experimental flow channel is a 1.3 m long vertical glass pipe with an internal diameter  $D_i=2.9$  mm. It is soldered to a conical glass hopper, with an opening angle of  $60^\circ$ , initially filled with grains which are then driven by gravity down the pipe (Fig. 1). The mass-flow rate can be varied by an adjustable stopcock located at the bottom end of the tube and measured using electronic computer controlled

\*Present address: LHMP/ESPCI (URA CNRS 857), 10 rue Vauquelin, 75231 Paris Cedex 05, France.

†Present address: Laboratoire de Physico-chimie, Pharmacotechnie, Biopharmacie (URA CNRS 1218), Faculté de pharmacie, Université Paris-Sud, 5 rue J. B. Clément, 92296 Chatenay-Malabry Cedex, France.

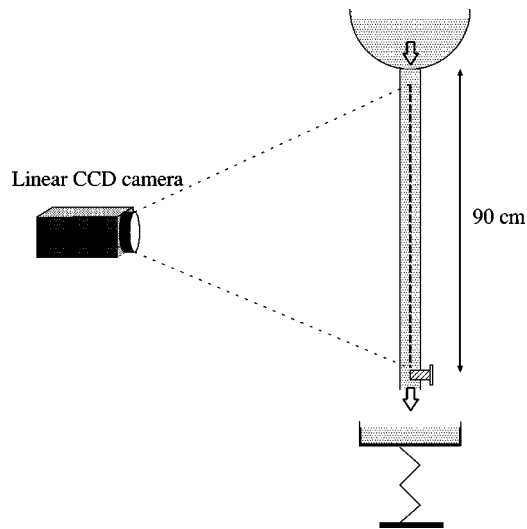


FIG. 1. Schematic view of the experimental setup.

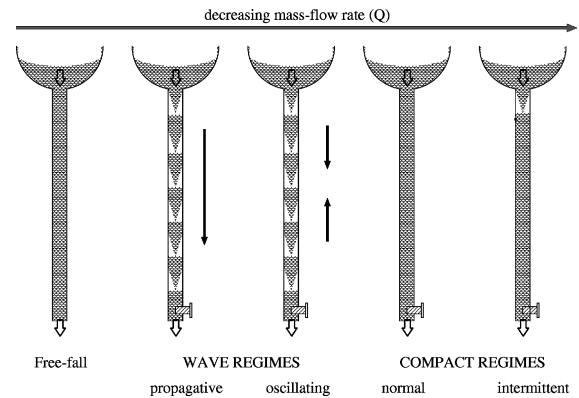
scales with a resolution of  $\pm 0.01$  g. In the present experiments we used glass beads of average diameter  $d_b = 125 \pm 30$   $\mu\text{m}$ . Choosing a transparent tube allows us to use optical techniques to characterize the different flow regimes. In order to enhance the contrast between regions of low and high granular density, the tube is illuminated from behind by a diffusing screen. The flow is visualized by a digital linear CCD camera (Fig. 1) mounted on a micrometric displacement assembly to allow for a precise angular and lateral alignment of the field of view with the flow tube. The camera is fully computer controlled and its sensitivity allows us to use both very short electronic obturation times and high acquisition frequencies (up to 2 kHz): this makes possible the analysis of very fast phenomena. Moreover, we may obtain a very good spatial resolution thanks to the 2048 pixels on the linear array of transducers. The reading of each of the transducer pixels is directly digitized and transmitted to the computer: this avoids distortions and noise introduced by the use of an intermediate video signal.

In the present study the acquisition frequency is equal to 200 Hz, which is markedly larger than the characteristic frequencies of the flow variations. Spatiotemporal diagrams obtained in this way are stored as numerical data arrays which are visualized directly using image processing programs. This representation allows us to study conveniently the motion of flow structures: it is then straightforward to determine the wavelength and propagation velocity of granular density variations as described in the following sections.

### III. QUALITATIVE ANALYSIS OF THE FLOW REGIMES

We now briefly review the main features of the flow regimes observed in the experimental setup and which are analyzed in detail in a previous paper [7]. These regimes are represented schematically in Fig. 2 for different flow rates and for given tube diameter and grain size distributions; their respective domains of existence are determined mostly by the flow rate and the degree of humidity. We summarize the main physical characteristics of these different regimes in Table I.

The highest mass-flow rates ( $Q_m \approx 10$  g/s) correspond to

FIG. 2. Schematic view of the various flow regimes observed as a function of the mass-flow rate  $Q_m$ .

a free-fall regime obtained with little or no constriction at the bottom of the pipe: the grain velocity is high (up to 2 or 3 m/s) and the compactness (granular volume fraction) is small (down to 15%). This flow regime is stationary so that the particle velocity is fairly constant with time and no significant particle density fluctuations occur: spatiotemporal diagrams did not display any clear features and were therefore not studied further in this regime. With a moderate constriction at the bottom of the flow tube and mass-flow rates  $Q_m$  ranging between 1.5 and 5 g/s, one observes density wave regimes: high compactness clogs (typically 55–60 %) are separated by low density “bubbles” inside which the grain dynamics is locally similar to the free-fall case. Such waves are only observed if the ratio  $D_t/d_b$  ranges between 6 and 30 (in the present experiments, it is of the order of 25); the degree of humidity  $H$  must also range between 40% and 70%. Excessive humidity results in clogging due to adhesive capillary forces between particles or between the particles and the tube wall; on the other hand, when air is too dry, electrostatic forces become excessive and also block the flow. The domains of  $H$  values discussed above get broader as  $Q_m$  increases. The velocity of compact clogs in the wave flow regime can be constant or oscillate periodically: the latter configuration is generally observed when humidity increases.

Finally, for  $Q_m$  between 0 and 1.5 g/s, the grain distribution is compact all along the flow tube. Such flows are observed for humidity contents and ratios  $D_t/d_b$  similar to those corresponding to the wave regimes. As for the latter, two different types of variations of the grain velocity with time are obtained. At the lower  $H$  values compatible with the flow, the velocity and the local compactness are constant with time. At higher water contents, on the contrary, periodic flow regimes are often observed: the flow from the hopper and in the upper part of the experimental tube is intermittent while the grain flow rate near the bottom outlet is only modulated and never goes to zero. For flow rates larger than 0.6 g/s, oscillations become very regular while a pulsating bubble with a low density of grains appears at the top of the flow tube. Another feature is the fact that the domain of observation of intermittent and oscillating flow regimes gets broader as experiments are repeated many times with a given batch of glass beads: this seems to be due to a progressive roughening of the bead surface due to their many collisions with other beads or with the tube walls.

In the next section we analyze by means of spatiotempo-

TABLE I. Summary of the different flow regimes and of the corresponding physical parameter values.

Flow regime	Mass flow rate (g/s)	Humidity (%)	Mean flow velocity (m/s)
Free fall	$5 < Q < 10$	$25 < H < 75$	$2 < V < 3$
Propagative waves	$2.5 < Q < 5$	$35 < H < 75$	$0.2 < V < 0.6$
Oscillating waves	$1.5 < Q < 2.5$	$35 < H < 75$	$0.1 < V < 0.3$
Compact	$0 < Q < 1.5$	$45 < H < 65$	$0 < V < 0.15$
Intermittent compact	$0 < Q < 1.5$	$45 < H < 65$	$0 < V < 0.15$

ral diagrams the dynamical features of the wave regimes and of the intermittent compact flow.

#### IV. WAVE FLOW REGIMES

##### A. Constant velocity waves

Figure 3 displays a spatiotemporal diagram corresponding to this regime in which high compact clogs separated by low density bubbles propagate at a constant velocity. The vertical axis represents distances measured along the flow tube with the top of the figure located at the junction between the tube and the hopper. The height of the diagram corresponds to a global length of 780 mm; it contains 1024 pixels so that the spatial resolution is 0.8 mm/pixel. The horizontal axis corresponds to time, increasing from left to right (the total width of the diagram represents a time lapse of 2.5 s). Since the tube is illuminated from behind, opaque clogs appear as dark zones while light regions represent bubbles.

As can be seen in Fig. 3, the wave regime does not get established right at the top of the tube although the first granular density fluctuations appear after a few mm: fully developed clogs require between 7 and 15 cm to build up. In the top part of the tube, grains fall under their own weight, only slowed down by friction with air. A second, important, feature is the fact that, outside a few wiggles, clogs follow

very closely parallel straight trajectories in the spatiotemporal diagram: such a fit is displayed in Fig. 3 by a continuous line. The slope  $V_p = \Delta z / \Delta t$  of these lines gives precisely the propagation velocity of the density waves (it is also equal to the velocity of the moving clogs once a stationary propagation regime has been reached). Figure 3 also shows that  $V_p$  is independent of height, at least in the range of  $z$  values displayed in the figure.

We have analyzed the dependence of these density waves on  $Q_m$  by comparing spatiotemporal diagrams similar to that of Fig. 3 and obtained at several  $Q_m$  values. A first qualitative observation is the fact that waves develop over markedly shorter distances as the flow rate decreases [for  $Q_m = 2.55$  g/s ( $V_p = 0.21$  m/s) clogs build up at distances of 4 to 8 cm below the hopper]. We have then analyzed the dependence on  $Q_m$  of the velocity values  $V_p$  obtained from these diagrams. The results are plotted in Fig. 4 (open squares).

These values have the same order of magnitude and the same global trend as previous measurements; these were realized on the same setup by computing  $V_p$  from the time shift  $\Delta t$  between the readings of local optical transparency sensors spaced by 23 mm. The discrepancy may be due to the fact that  $\Delta t$  was taken equal to the time lapse corresponding to the maximum of the cross-correlation function between the two signals. This introduces a significant uncertainty since the peak has a finite width, and since the two signals contain uncorrelated high frequency components. The computation of  $V_p$  from the spatiotemporal diagrams is then expected to be more reliable; in addition, it uses infor-

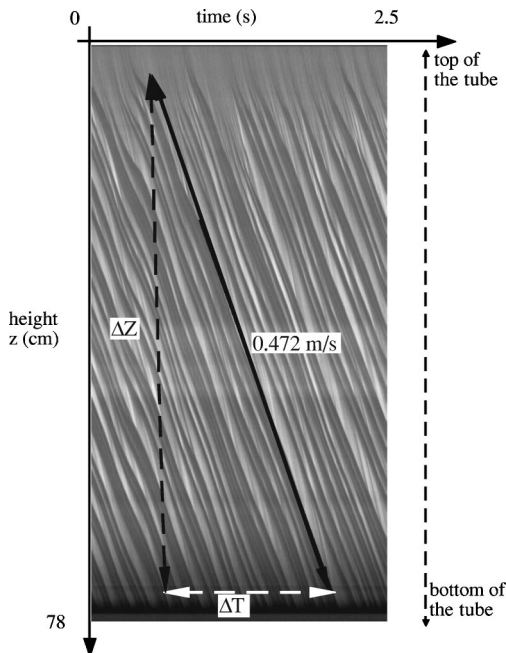


FIG. 3. Spatiotemporal diagram obtained in the propagative wave regime ( $Q_m = 4.25$  g/s). The oblique continuous line corresponds to  $V_p = 0.47$  m/s.

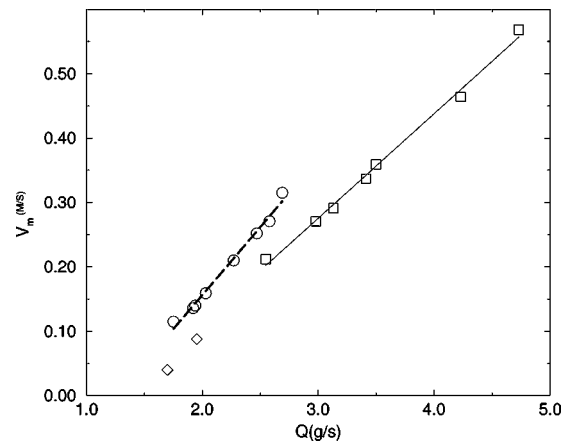


FIG. 4. Variations of the wave velocity  $V_p$  as a function of the mass-flow rate  $Q_m$ ; ( $\square$ ) spatiotemporal diagrams for constant velocity waves; ( $\diamond$ ) spatiotemporal diagrams for oscillating waves; ( $\circ$ ) cross-correlation between optical sensors spaced by 23 mm.

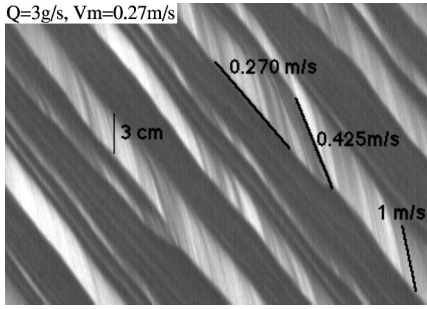


FIG. 5. Enlarged spatiotemporal diagram of a wave flow ( $Q_m = 3.0$  g/s,  $V_p = 0.27$  m/s). Vertical height:  $\Delta z = 23$  cm; time interval:  $\Delta t = 1.5$  s.

mation collected over the full length of the field of view and not only at two nearby measurement points. The dependence of  $V_p$  on  $Q_m$  measured in this way can be approximated by the relation (continuous straight line on Fig. 4)

$$V_p = 0.162(Q_m - 1.4) \quad (1)$$

in which  $V_p$  is written in m/s and  $Q_m$  in g/s. We observe that an extrapolation of this relation predicts that  $V_p$  would go to zero for a finite flow-rate value  $Q_m = 1.4$  g/s. This result reflects the fact that the average grain velocity is markedly larger than  $V_p$  so that grains have a downward motion relative to the wave system. Individual grains move down from the upper boundary towards the lower end of a clog and then into the bubble immediately below. There, they are accelerated by gravity until they reach the upper boundary of the next clog where they get abruptly slowed down. Such fast moving species may be observed in the detailed structure of the wave flow system displayed in Fig. 5. They appear as parallel striations between dark high compactness zones. Individual grains are probably too small to be directly observable although, due to the low local compactness, their distance is of the order of the pixel size; thus, striations are probably associated to small grain clusters. Striations have a downward curvature in the upper part in agreement with the expectation that grains accelerate as they move away from the clogs. After a few cm, they reach a velocity of the order of 1 m/s (slope of the continuous line drawn in the right side of the figure). This velocity can be roughly estimated theoretically by assuming a free fall motion inside bubbles. The initial velocity  $V_0$  of particles leaving a clog in the flow of Fig. 5 verifies

$$Q_m = \frac{\pi D_t^2}{4} \rho_g c_c V_0 \quad (2)$$

in which  $\rho_g$  is the density of glass (typically  $2.45 \times 10^3$  kg/m<sup>3</sup>) and  $c_c$  the compactness of the clogs which can be assumed to be of the order of 0.6. Thus  $V_0 = 0.3$  m/s and the velocity  $V_f$  after falling a distance  $\delta z$  verifies

$$V_f = \sqrt{V_0^2 + 2g\delta z}. \quad (3)$$

Taking  $\delta z \approx 0.05$  m as estimated from Fig. 5 in the absolute reference frame, one obtains  $V_f \approx 1$  m/s. This is in reason-

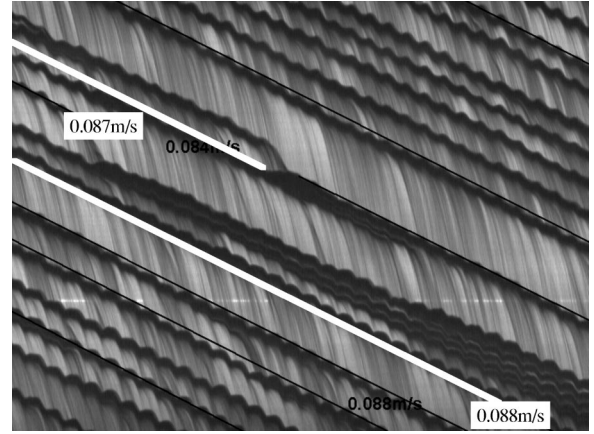


FIG. 6. Spatiotemporal analysis of a small amplitude oscillating wave flow ( $Q_m = 1.95$  g/s,  $V_p = 0.088$  m/s). Vertical extent  $\Delta z = 60$  cm. Time interval  $\Delta t = 4.3$  s.

able agreement with the experimental estimation, particularly taking into account the fact that friction with air has been neglected.

The enlarged view of Fig. 5 also allows us to examine the detailed structure of the high compact zones: they appear as superpositions of smaller clogs,  $\sim 1$  cm thick, which remain together without collapsing into a single, larger, zone. The number of elementary clogs in a cluster increases at lower flow rates while their size remains the same. One also observes that clog clusters do not always remain invariant: some small clusters are observed to disintegrate and the corresponding elementary clog falls down onto the nearest lower cluster. An example of such an event is displayed in the right side of Fig. 5. The falling velocity is of the order of 0.4 m/s (marked by a continuous line)—this value is slower than the free fall velocity because of the stronger effect of air friction enhanced by the high local compactness. Individual clogs may also move from one cluster to another.

This detailed spatiotemporal analysis of the constant velocity wave regime demonstrates therefore that it corresponds to a state of dynamical equilibrium. Particle flow is always present in such a system: it takes place through the motion of individual particles falling in low density zones but also through the exchange of elementary clogs between high compact zones.

## B. Low amplitude oscillating wave regime

At lower flow rates, but still in the wave flow regime, one may observe oscillations of the whole set of clogs and bubbles superimposed over a mean drift. Figure 6 represents such a flow regime for which the frequency of the oscillations is of the order of 7 Hz and their amplitude is high enough to induce upward motions of the clogs. This low characteristic oscillation frequency can be understood by considering the granular flow as a diphasic system with a high compressibility (that of air) and a high density (of the order of the density of glass multiplied by the global mean compactness of the flow). By computing the sound velocity in such a system, one obtains very low values of the order of 20 m/s. Let us assume a quarter-wave resonance with a minimum amplitude of the pressure oscillations at the top of the wave system and a maximum of the bottom; we obtain by

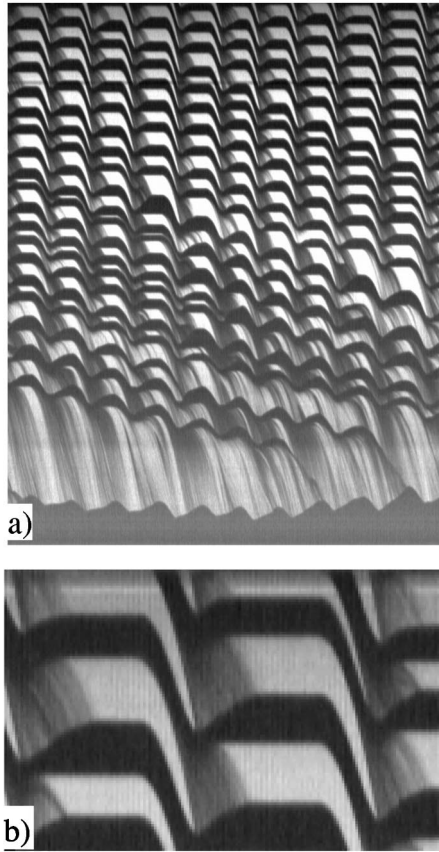


FIG. 7. (a) Spatiotemporal diagram obtained in a high amplitude oscillating regime ( $Q_m = 1.77$  g/s). Time interval displayed:  $\Delta t = 2.25$  s. Vertical extension  $\Delta z = 75$  cm. (b) Enlarged view of the upper part of the spatiotemporal diagram.

taking  $\lambda/4 = 1$  m (the height of the wave flow region) a resonance frequency  $\nu = 5$  Hz of the same order of magnitude as the experimental value. Aside from the oscillations, the general features of the flow are the same as in the constant velocity wave regime; the mean velocity of the clogs is constant along the flow and its value  $V_p \approx 0.09$  m/s verifies Eq. (1). Striations are always present inside the “bubble” regions, indicating that granular flow through the clogs remains nonzero. One should finally notice that the typical size of the clogs in this regime is always of the order of 1 cm.

### C. Large amplitude oscillations: a stick-slip process

In some cases, generally at low flow rates ( $1.5 < Q_m < 2$  g/s), the amplitude of the oscillations may be so large that intermittent blockages of the flow occur. A spatiotemporal diagram corresponding to this case for a flow rate  $Q_m = 1.7$  g/s is displayed in Fig. 7(a). This diagram differs globally very strongly from that of Fig. 6 and its features vary very much from the top to the bottom.

Flow characteristics in the lower part are similar to those observed in Fig. 6. Clogs move with a modulated drift velocity of mean value  $V_p \approx 0.04$  m/s in fair agreement with Eq. (1) and no complete blockage of the flow occurs. On the other hand, the modulation frequency is of the order of 4.5 Hz, markedly smaller than for small amplitude oscillations: this frequency is forced by upstream flow variations. At the

bottom as well as at the top of the tube, clogs have the same average size  $\lambda \approx 1$  cm as in the other flow regimes, confirming that this length is selected independently of the mass-flow rate.

The dark zone at the bottom of the figure represents the upper part of a long, high compact plug extending down to the outlet end of the tube: its wiggly upper boundary implies that the grain flow rate coming from the upper zones is significantly modulated.

Flow variations in the upper part of the tube, on the other hand, are more clearly visualized in the enlarged view displayed in Fig. 7(b). Flow is completely blocked during a significant part of the time during which boundaries between clogs and bubbles appear as horizontal segments. In these same time intervals, regions of the diagram associated to bubbles are almost white—implying that they do not contain any grains—this confirms that the granular flow rate is zero at these times.

We observe that the motion of the clog-bubble system takes place through a series of downward jumps during which no grain flow is visible inside bubbles. The clog velocity during the jumps is of the order of 0.6 m/s. Right after the jumps, grains start to fall through the bubbles as can be seen both from the darker color of the bubble regions and from the upward rebound of the clog boundaries. Finally the flow stops and the system remains completely motionless until the next downward motion of the grain clogs occurs. An interesting observation is the fact that, in the upper part of the tube, the distribution of clogs and bubbles remains almost the same from one jump to the next: each clog is just replaced by the one located just above. The whole process resembles stick-slip motions observed in many friction phenomena: the fact that grains are motionless during a significant part of the time must result from solid forces between the clog and the tube walls, large enough to balance the pressure gradients and the weight of the grains. We finally observe that, in the upper region of the tube, compact clogs have the same height  $\Delta z = 10\text{--}14$  mm as in the constant velocity wave regime of Fig. 5: elementary clogs are, however, isolated instead of clustering together as in Fig. 5. In the bottom part of the flow, one observes a few events in which two clogs coalesce into a larger one. They join progressively due to their small velocity difference; this is quite different from the case of Fig. 5 in which some clogs abruptly start to fall towards the next lower one.

## V. COMPACT INTERMITTENT REGIME

### A. Spatiotemporal experimental observations

For tighter outlet constrictions such that  $Q_m < 1.5$  g/s, the wave regime disappears and the tube is almost completely filled with a compact grain packing: flow is stationary in some cases but, for degrees of humidity  $50\% < H < 65\%$ , it is frequently time dependent. More precisely, flow is continuous (although fluctuating) at the outlet end while it is intermittent at the top of the tube. Moreover, a pulsating bubble appears just below the hopper but does not propagate down the tube.

Several of these features are analogous to those observed in the “ticking hourglass” experiment [24] in which a periodic intermittent granular flow is observed between two

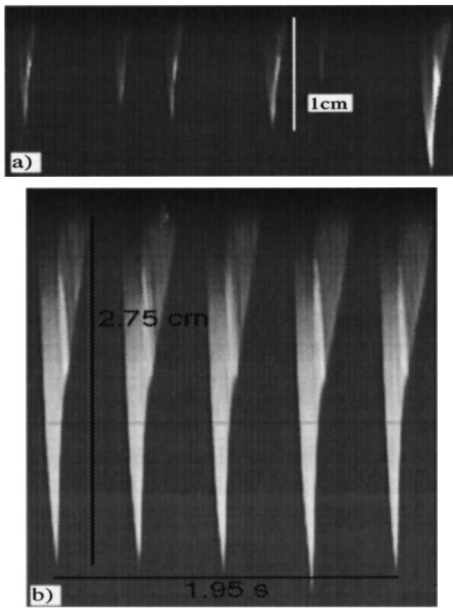


FIG. 8. Spatiotemporal diagram of low density region at top of the flow tube in the intermittent compact regime. (a) Time averaged granular mass-flow rate  $Q_m = 0.4$  g/s, vertical range  $\Delta z = 1.5$  cm, time interval  $\Delta t = 9$  s. (b)  $Q_m = 1.05$  g/s,  $\Delta z = 3.3$  cm,  $\Delta t = 2.3$  s.

sealed glass volumes connected by a narrow constriction. A small pulsating bubble is also observed in the granular packing in the upper reservoir. However, the ‘‘ticking hourglass’’ phenomenon is localized over a small volume while, in our case, large velocity fluctuations are observed over distances of several cm and sizable pressure variations may be induced.

In our experiments, the different time variations of the flow rate at the top and at the bottom of the experimental tube imply that the mass of grains inside the tube is not constant: the grain compactness must therefore vary with time (and probably with distance). In both types of regimes, spatiotemporal diagrams do not display visible features along most of the tube length since the compact packing is opaque and light cannot be transmitted through it. All measurements were therefore performed in a 4 cm high region just below the hopper where the partly transparent pulsating bubble is located. This allows us to obtain a better spatial resolution which is in this case  $40 \mu\text{m}/\text{pixel}$ . The transverse resolution is of the same order of magnitude so that only the center part of the flow is analyzed.

Figures 8(a) and 8(b) display such spatiotemporal diagrams corresponding, respectively, to flow rates of 0.40 and 1.05 g/s; light zones correspond to the pulsating bubbles. For flow rates below 0.7 g/s, flow fluctuations [as can be inferred from the diagram of Fig. 8(a)] are irregular and the height and lifetime of the pulsating bubble are also variable. At flow rates larger than 0.7 g/s, on the contrary, flow fluctuations are very periodic [Fig. 8(b)] and the maximum size of the bubble is very nearly constant from one pulsation to the next. The detailed flow sequence at the top of the pipe may be analyzed by combining high resolution information from the diagram to direct videotape observations on the various parts of the tube, allowing us to detect whether grains are moving or at rest.

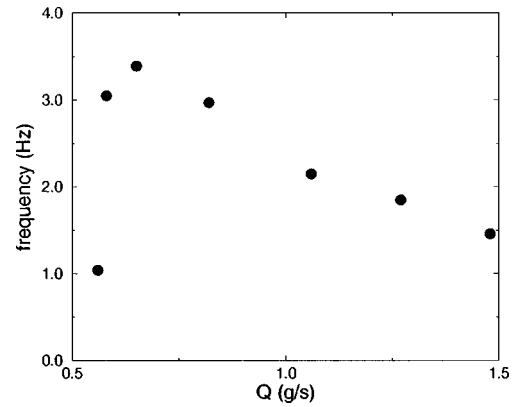


FIG. 9. Evolution of the pulsation frequency as a function of the granular mass-flow rate in the intermittent regime.

Starting during a phase of the cycle at which the grain packing is at rest at the top of the tube and in the hopper, flow first restarts globally in these zones (it never stops completely in the lower part of the tube). The bubble appears only in a subsequent phase initiated by a localized reduction of the flow rate at the outlet of the hopper. Granular motion remains at first unchanged in the lower sections of the tube and a low density region appears while grains still fall through it as shown by fine striations in the diagram: this phase corresponds to the downward sloping part of the contour of light zones in Fig. 8. Then, granular velocity decreases and goes to zero below the bubble while grains falling from the hopper fill up the bubble. This phase corresponds to the rising part of the contour of the light zones in Fig. 8 and lasts typically for 0.2 s. Flow stops after the bubble is completely filled and the cycle is then ready to start again. An interesting—although unaccounted for—feature is the narrow lighter colored stripe marking a temporary reduction of granular flow from the hopper: this variation is confirmed by the corresponding local slope reduction in the rising part of the contour.

Before discussing possible mechanisms for these blockage effects, we now analyze quantitatively the dependence of the frequency  $f_b$  of the pulsations and of the characteristic bubble length  $l_b$  on the grain flow rate. Both parameters can be determined with a good precision from the spatiotemporal diagrams of Fig. 8 ( $l_b$  is taken equal to the average maximum height of the light colored zones marking the bubbles).

Figure 9 displays the dependence of  $f_b$  on  $Q_m$ . The effective frequency decreases quite abruptly below the threshold flow rate ( $Q_m \approx 0.65$  g/s) for observing constant period fluctuations (only one data point is plotted in this range since the period is too variable at lower flow rates). Above 0.65 g/s,  $f_b$  decreases progressively with the flow rate—possibly due to the larger amplitude of the perturbations induced by the intermittency effect. Figure 10 displays the dependence of the length  $l_b$  of the pulsating bubble on  $Q_m$ .

$l_b$  increases steadily and roughly linearly with  $Q_m$  (although the variation seems to level off at very low flow rates): the length of the bubbles increases almost fourfold between the lowest and highest values of  $Q_m$  investigated. Since the characteristic velocities for opening and filling back the pulsating bubbles do not seem to vary as much with

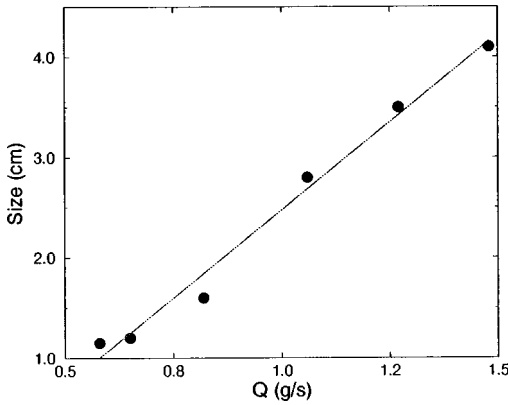


FIG. 10. Variation of the pulsating bubble length  $l_b$  as a function of the granular mass-flow rate  $Q_m$ .

the flow rate, we can conclude that the increase of  $l_b$  and the decrease of  $f_b$  are directly related.

### B. Discussion of intermittency and stick-slip effects

In both the high amplitude oscillating wave regime and the intermittent compact flow, the grain velocity cancels out during a fraction of the time, at least in the upper parts of the flow. This implies that solid friction forces between the grains and the walls are large enough to balance the weight of the grains already reduced by hydrodynamic forces. A simple classical approach of these forces is represented by Jansen's model [25,4]. In the following, the vertical stress on the beads at a given level in a grain packing will be called  $\sigma_v$ ;  $\sigma_v$  is assumed to create a normal horizontal stress  $\sigma_h = K\sigma_v$  on the side walls,  $K$  being the redirection coefficient.  $\sigma_h$  induces, in turn, a vertical friction force  $\sigma_f = \mu_s\sigma_h$  in the direction opposite to displacement ( $\mu_s$  is the static friction coefficient). The total friction force  $\delta F_{\text{friction}}$  over a slice of tube of length  $\delta h$  is finally

$$\delta F_{\text{friction}} = 2\pi D_t K \mu_s \sigma_v \delta h. \quad (4)$$

In a grain packing at rest inside a tube there is an exact balance between the weight of the column (and hydrodynamic forces if there is a fluid flow), friction forces on the walls, and stresses applied to the top and bottom sections of the packing. However, friction forces appear (and  $K$  is non-zero) only provided the grain density is large enough so that forces are transmitted through solid contacts between the grains. One may also expect that these friction forces will increase with the ambient humidity.

In the intermittent compact regime, granular flow gets blocked at some height inside the tube due to a local increase of the compactness; this may result from a pressure gradient distribution pushing the grains together in a given zone of the flow. Grains pile up above the blocking point but, above a small screening length, their weight is exactly balanced by the local friction forces and no longer affects the lower layers in the column. In this case, flow cannot be restarted by increasing forces applied at the top of the packing since they are not transmitted to the bottom: a new flow cycle may only

be initiated instead from decompaction starting near the blocking point and propagating upwards once pressure gradients inducing the blockage have relaxed.

In the stick-slip wave regime, clog blockages result from similar mechanisms but compact grain packings are much shorter so that no force screening effects can be developed. Pressure gradients along the flow will probably play an important part in controlling the stick-slip motion of the clogs.

Another possible application of Jansen's model to the present problem is the evaluation of the vertical extension of the compact clog in the constant velocity wave regime. The typical vertical size  $\lambda \approx 1$  cm of the clogs may indeed be interpreted as the minimum length for a compact granular zone to propagate without disintegrating:  $\lambda$  should therefore be related to the characteristic length over which granular interaction forces build up inside a grain packing. Let us first take the classical problem of a tube closed at its bottom end and filled with a grain packing of height  $h$ . Using Eq. (4), one finds that the resultant pressure  $p_v$  on the bottom section due to the balance between the weight of the grains and the friction forces verifies

$$p_v = \rho g \frac{D}{4K\mu_s} (1 - e^{-(4K\mu_s/D)h}). \quad (5)$$

Equation (5) introduces a characteristic screening length  $h_{cs} = D/4K\mu_s$  over which pressure reaches the saturation value  $p_s = \rho g D/4K\mu_s$ .

This value cannot be used directly to estimate  $\lambda$  since, for the constant velocity waves discussed in Sec. IV A, clogs are never completely at rest (in contrast with the cases of the oscillating regime and the intermittent compact flow). The static coefficient  $\mu_s$  is therefore not appropriate and should be replaced by a dynamic friction coefficient  $\mu_d$ . The characteristic screening length suitable for the problem is then  $h_{cd} = D/4K\mu_d$ .

Assuming that  $h_{cd}$  and  $\lambda$  are of the same order of magnitude, one obtains  $K\mu_s \approx 0.075$ . Taking  $K \approx 0.55$ —close to the value  $K_{\text{CTP}} = 0.58$  for a compact triangular packing—we obtain  $\mu_s \approx 0.125$  for the dynamic friction coefficient. This is somewhat lower than the static coefficient value  $\mu_s \approx 0.2$  usually encountered in such materials. This difference is not surprising since clogs are still strongly fluidized in the constant velocity wave regime; they may be expected to have smaller interactions with the walls than a packing at rest. For the same reasons, the coefficient  $K$  should also be smaller than  $K_{\text{CTP}}$ : this would give a value of  $\mu_d$  closer to  $\mu_s$ .

## VI. CONCLUSION

The spatiotemporal analysis of granular pipe flows presented in the present paper has demonstrated several new features of the various flow regimes. It has been, in particular, possible to analyze in detail the transition—depending on the flow rate and the humidity—between constant velocity waves and periodic, stick-slip type, regimes in which clogs and bubbles move by discontinuous steps. Spatiotemporal diagrams also allow us to analyze small scale details of these wave flow regimes, such as the motion of grains in low den-

sity zones and the clustering or coalescence of high compactness clogs. The compact intermittent regime involves periodic granular flow variations right at the top of the flow tube and farther below: these sequences are better understood by looking at spatiotemporal diagrams of the pulsating bubble at the top of the flow tube.

An important issue in these phenomena is the influence of boundary conditions at the top and bottom of the tube on the structure and dynamical features of the flow. We observed that time dependent effects observed in the various flow regimes are often localized in the upper sections of the flow. In the wave regime, the long compact plug built up above the outlet damps out flow rate and density fluctuations: the aperture and geometry of the restriction at the outlet seems therefore to control the mean characteristics of the flow rather than its instantaneous dynamic behavior. The same damping effect is observed in the intermittent compact regime where flow fluctuations are much stronger in the top part of the flow than at the outlet.

In the case of the upper boundary just below the hopper, strong velocity variations are mostly observed for intermittent compact flows. In the stationary and low amplitude oscillating wave regimes, grains flow continuously from the hopper and retain a free-fall-like dynamics for some distance until clogs build up. We believe therefore that time dependent features of the flow are little influenced by the outlet and that the inlet boundary plays a key part essentially in intermittent compact flows.

Another important parameter of this type of granular flows is the interaction forces between the flow and the tube walls. Both in the stick-slip waves and intermittent compact regimes, grains are completely motionless (at least in some regions of the flow) during a significant fraction of the time. As discussed above, this requires that solid forces appear between the grains and the tube walls and inside the grain packing itself. In this respect, such granular flows may display mechanical characteristics corresponding to solid or

fluid materials depending on the flow regime and on the regions of the flow. Understanding the onset of solid forces and the propagation of grain compaction and decompaction requires the determination of the local compactness; high resolution capacitance measurements represent a possible practical approach which is presently investigated in our laboratory.

Ambient humidity is also a key factor determining the dynamical characteristics of such flows: depending on its degree, capillary, or, on the contrary, electrostatic forces may completely block the flow in extreme cases. In others, they favor the appearance of intermittent, stick-slip-wise or oscillating flow regimes. Complex behaviors are often more easily observed at the boundary between different types of flows (for instance, between the wave and the compact regimes). Good humidity control is thus very important to obtain well defined and stable flow regimes but the roughness and cleanliness of the bead surface may also play a significant part.

One finally notes that the interest of these experimental approaches is not limited to small scale granular flows; they can also be used in larger scale configurations provided transparent flow sections are available. Such techniques can also be applied with profit to many other types of dispersed flows such as sedimenting particles, fluidized beds, and liquid-liquid or liquid-gas diphasic flows.

#### ACKNOWLEDGMENTS

We thank Professor H. J. Herrmann and Professor E. J. Hinch for helpful discussions. We also thank the GDR "Physique des Milieux Hétérogènes Complexes" for partial support of this project, P. Petitjeans and J. E. Wesfreid for giving us the opportunity to use the linear CCD camera, and G. Chauvin for his help in the realization of the optical measurement setup. The Laboratoire Fluides Automatique et Systèmes Thermiques is associated with CNRS and with the Pierre et Marie Curie and Paris-Sud Universities (UMR No. 7608).

- 
- [1] H. M. Jaeger and S. R. Nagel, *Science* **255**, 1523 (1992).
- [2] K. Rietema, *The Dynamics of Fine Powders* (Elsevier Science Publishers, New York, 1991).
- [3] R. M. Nedderman, *The Statics and Dynamics of Granular Materials* (Cambridge University Press, Cambridge, England, 1992).
- [4] J. Duran, *Sables Poudres et Grains, Introduction à la Physique des Milieux Granulaires* (Eyrolles Sciences Publisher, Paris, 1997).
- [5] S. Horikawa, A. Nakahara, T. Nakayama, and M. Matsushita, *J. Phys. Soc. Jpn.* **64**, 1870 (1995).
- [6] O. Moriyama, T. Isoda, N. Kuroiwa, M. Kanda, I. Rafols, and M. Matsushita, *J. Phys. Soc. Jpn.* **67**, 1616 (1998).
- [7] T. Raafat, J. P. Hulin, and H. J. Herrmann, *Phys. Rev. E* **53**, 4345 (1996).
- [8] T. Raafat, J. P. Hulin, and H. J. Herrmann, in *Traffic and Granular Flow*, Proceedings of the 1st Workshop on Traffic and Granular Flow (Jülich, 9–11 October, 1995), edited by D. E. Wolf, M. Schreckenberg, and A. Bachem (World Scientific, Singapore, 1996), p. 317.
- [9] J. Lee, *Phys. Rev. E* **49**, 281 (1994).
- [10] G. W. Baxter, R. P. Behringer, T. Fagert, and G. A. Johnson, *Phys. Rev. Lett.* **62**, 2825 (1989).
- [11] C. T. Veje and P. Dimon, *Phys. Rev. E* **54**, 4329 (1996).
- [12] H. J. Herrmann, in *Mobile Particulate Systems*, Proceedings of the NATO Advanced Study Institute on Mobile Particulate Systems, Cargese, Corsica (France), July 4–15, 1994, Vols. 2 & 7 of *NATO Advanced Study Institute Series E: Applied Science*, edited by E. Guazzelli and L. Oger (Kluwer Academic Publishers, Dordrecht, 1995), p. 281.
- [13] S. B. Savage, *J. Fluid Mech.* **244**, 109 (1992).
- [14] C. H. Wang, R. Jackson, and S. Sundaresan, *J. Fluid Mech.* **342**, 179 (1997).
- [15] C. K. K. Lun, S. B. Savage, D. J. Jeffrey, and N. Chepur, *J. Fluid Mech.* **140**, 223 (1984).
- [16] J. Lee and M. Leibig, *J. Phys. I* **4**, 507 (1994).
- [17] M. Leibig, *Phys. Rev. E* **49**, 184 (1994).
- [18] M. J. Lighthill and G. B. Whitham, *Proc. R. Soc. London, Ser. A* **229**, 281 (1955); **229**, 317 (1955).
- [19] T. Musha and H. Higuichi, *Jpn. J. Appl. Phys.* **15**, 1271 (1976).

- [20] K. Nagel and M. Schreckenberg, *J. Phys. I* **2**, 2221 (1992).  
[21] G. W. Baxter and R. P. Behringer, *Phys. Rev. A* **42**, 1017 (1990).  
[22] G. Peng and H. J. Herrmann, *Phys. Rev. E* **49**, R1796 (1994).  
[23] T. Pöschel, *J. Phys. I* **4**, 499 (1994).  
[24] T. Le Pennec, K. J. Málóy, A. Hansen, M. Ammi, D. Bideau, and X. L. Wu, *Phys. Rev. E* **53**, 2257 (1996).  
[25] H. A. Jansen, *Z. Vereins Deutsch Ing.* **39**, 1045 (1895).